20. J. F. Stebbins, J. B. Murdoch, I. S. E. Carmichael, A. Pines, *Phys. Chem. Mineral.* **13**, 371 (1986); G. L. Hovis *et al.*, *Eos* **70**, 353 (1989).
21. H. H. Ulbrich and D. R. Waldbaum, *Geochim. Cosmochim. Acta* **40**, 1 (1976).
22. M. S. Ghiorso and I. S. E. Carmichael, *Contrib. Mineral. Petrol.* **90**, 121 (1985).
23. J. F. Stebbins, I. S. E. Carmichael, L. K. Moret, *ibid.* **86**, 131 (1984).
24. J. Klinowski *et al.*, *Nature* **330**, 56 (1987); J. F. Stebbins, *ibid.*, p. 13. Violations of strict aluminum avoidance are more common in aluminosilicates containing higher field-strength interstitial cation such as $Ca^{2+}$ and $Mg^{2+}$; A. Putnis, in *Physical Properties and Thermodynamic Behavior of Minerals*, E. K. H. Salje, Ed. (Reidel, Dordrecht, 1988); B. L. Phillips *et al.*, *Eos* **70**, 351 (1989).
25. J. F. Stebbins, paper presented at the 30th Experimental NMR Conference, Asilomar, CA, April 1989; ———, I. Farnan, E. Williams, in preparation.
26. B. L. Sheriff and H. D. Grundy, *Nature* **332**, 819 (1988).
27. B. L. Phillips, R. J. Kirkpatrick, G. L. Hous, *Phys. Chem. Mineral.* **16**, 262 (1988).
28. B. C. Bunker *et al.*, *Phys. Chem. Glasses* **29**, 106 (1988).
29. J. A. Peck, I. Farnan, J. F. Stebbins, *Geochim. Cosmochim. Acta* **52**, 3017 (1988).
30. E. Schneider, J. F. Stebbins, A. Pines, *J. Non-Cryst. Solids,* **89**, 371 (1986).
31. A. Samosen, E. Lippmaa, A. Pines, *Mol. Phys.* **65**, 1013 (1988).
32. B. F. Chmelka *et al.*, *Nature* **339**, 42 (1989).
33. S. H. Risbud *et al.*, *J. Am. Ceram. Soc.* **70**, C10-C12 (1987).
34. R. Dupree, D. Holland, M. G. Mortuza, *Nature* **328**, 416 (1987).
35. S. M. Rigden, T. J. Ahrens, E. M. Stolper, *J. Geophys. Res.* **93**, 367 (1988).
36. C. M. Scarfe *et al.*, in *Magmatic Processes: Physicochemical Principles*, B. O. Mysen, Ed. (Geochemical Society, University Park, PA, 1987), pp. 59–68.
37. M. E. Fleet *et al.*, *Geochim. Cosmochim. Acta* **48**, 1455 (1984); M. F. Hochella, Jr., and G. E. Brown, Jr., *ibid.* **49**, 1137 (1985); P. F. McMillan and C. M. Graham, in *Progress in Experimental Petrology*, C. E. Ford, Ed. (National Environmental Research Council, London, 1981), pp. 112–115; B. O. Mysen *et al.*, *Neues. Jahrb. Mineral. Abh.* **147**, 281 (1983). Vibrational spectra of glasses at high pressure and room temperature have indicated increases in Si coordination with pressure [Q. Williams and R. Jeanloz, *Science* **239**, 902 (1988)].
38. E. Ohtani, F. Taulelle, C. A. Angell, *Nature* **314**, 78 (1985).
39. X. Xue, J. F. Stebbins, M. Kanzaki, R. C. Tronnes, *Science*, in press; J. F. Stebbins, P. McMillan, *Am. Mineral.*, in press.
40. R. F. Pettifer *et al.*, *J. Non-Cryst. Solids* **106**, 408 (1988).
41. J. B. Murdoch, J. F. Stebbins, I. S. E. Carmichael, *Am. Mineral.* **70**, 332 (1985).
42. J. F. Stebbins, *Nature* **330**, 465 (1987).
43. ———, *J. Non-Cryst. Solids* **106**, 359 (1988).
44. P. Richet, *Geochim. Cosmochim. Acta* **48**, 471 (1984); C. A. Angell, in *Relaxation in Complex Systems*, K. L. Ngai and G. B. Wright, Eds. (Office of Naval Research, Washington, DC, 1985), pp. 3–12.
45. M. E. Brandriss and J. F. Stebbins, *Geochim. Cosmochim. Acta* **52**, 2659 (1988).
46. For example, B. H. W. S. De Jong, K. D. Keefer, G. E. Brown, Jr., C. M. Taylor, *Geochim. Cosmochim. Acta* **45**, 1291 (1981).
47. M. S. Ghiorso *et al.*, *Contrib. Mineral. Petrol.* **84**, 107 (1983).
48. E. M. Stolper, *Geochim. Cosmochim. Acta* **46**, 209 (1982).
49. H. Eckert, J. P. Yesinowski, L. A. Silver, E. M. Stolper, *J. Phys. Chem.* **92**, 2055 (1988); H. Eckert, J. P. Yesinowski, E. M. Stolper, T. R. Stanton, J. Holloway, *J. Non-Cryst. Solids* **93**, (1987); I. Farnan, S. C. Kohn, R. Dupree, *Geochim. Cosmochim. Acta* **51**, 2869 (1987).
50. S. Brawer, *Relaxation in Viscous Liquids and Glasses* (American Ceramic Society, Columbus, OH, 1985); M. F. Hochella, Jr., and G. E. Brown, Jr., *Geochim. Cosmochim. Acta* **48**, 2631 (1984).
51. J. F. Stebbins *et al.*, *Nature* **314**, 250 (1985).
52. S.-B. Liu *et al.*, *Phys. Chem. Minerals* **15**, 155 (1987); S.-B. Liu, J. F. Stebbins, E. Schneider, A. Pines, *Geochim. Cosmochim. Acta* **52**, 527 (1988).
53. I. Farnan and J. F. Stebbins, *Eos* **69**, 1482 (1988); in preparation.
54. J. F. Stebbins, in *Spectroscopic Methods in Mineralogy and Geology*, F. C. Hawthorne, Ed. (Mineralogical Society of America, Washington, DC, 1988), pp. 405–430.
55. D. B. Dingwell and S. L. Webb, *Phys. Chem. Mineral.* **16**, 508 (1989).
56. We acknowledge the support of National Science Foundation grants EAR 8707175 and EAR 85-53024 and the continued assistance of D. R. Spearing. The spectrometer used for much of the work described here was funded by the NSF, the Pew Foundation, and a gift from Varian Associates.

# The Applications of Closure Phase to Astronomical Imaging

T. J. CORNWELL

**Closure phase is a number measured by triplets of Michelson interferometers that is completely independent of certain types of otherwise severe instrumental errors. In the 30 years since closure phase was invented, it has been applied to a diverse number of different problems in astronomical imaging. Methods based on the closure phase now allow imaging of complex objects in the presence of severe aberrations and are vital to the success of modern, high-resolution astronomical imaging both at radio and at optical wavelengths. Over the past 10 to 15 years, the concept of closure phase has been extended and generalized. One of the most important advances has been the development of automatic or self-calibration techniques. This article reviews closure phase methods and some of the many spin-offs and related ideas.**

A MICHELSON INTERFEROMETER CAUSES THE LIGHT COLlected at two mirrors to undergo wave interference at a common focus (see Fig. 1). Interference fringes will be seen with a contrast that depends on the structure of the light source. A change in the optical path length in one arm (such as occurs if mirror A is moved to position A′) will shift the fringe position. This fringe position is known as the fringe phase, and one can measure it by rapidly modulating a mirror between two different positions corresponding to a change in the delay of the signal by $\lambda/4$, where $\lambda$ is wavelength. The fringe phase contains useful information about the structure of the source, but it is nearly always corrupted by either mechanical instabilities or path length changes above the mirrors due to atmospheric turbulence. Furthermore, rapid changes in the fringe phase lead to washing out of the fringes, an effect that ultimately limited Michelson's original observations.

Although Michelson first demonstrated interferometry at optical wavelengths, the sustained development of his technique was substantially easier at radio wavelengths and was pursued vigorously in the late 1940s and early 1950s by a number of groups. The principal reason for preferring radio wavelengths was that the radiation could be amplified and detected easily with the electronics technology developed in World War II. Ryle's phase-switching interferometer (*1*) was used for cosmological studies and for studies of the structure of radio sources. Modern radio telescopes consist of arrays of phase-switching interferometers connected to sample the coherence function of the electromagnetic field. From such samples, it is possible to image complex objects. However, even in radio interferometry, the difficult problem of measuring the phase of the interference fringes often remains. Fortunately, as I will show in this article, in many

The author is at the National Radio Astronomy Observatory, Socorro, NM 87801.

**Fig. 1.** A simple Michelson interferometer. The light collected at the two outlying mirrors is brought to a common focus where fringes are observed. A shift of the mirror from A to A′ in one arm will shift the fringes as shown.

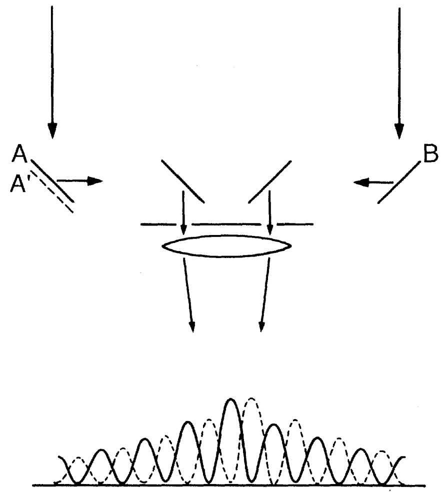


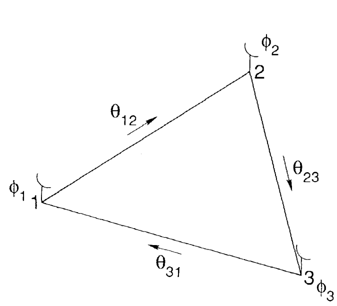


**Fig. 2.** Closure phases. The element-based errors $\phi_i$ vanish in the sum of the observed phases around a loop. This is Jennison's closure phase.

cases one can bypass this problem by using, instead, Jennison's closure phase (*2*). Imaging methods based on the closure phase have spread to optical and infrared astronomy and are now vital for many modes of high angular resolution astronomical imaging.

## Closure Phase in Radio Interferometry

A more sophisticated variant of Michelson's interferometer, the multiplying or phase-switching interferometer (*3*), measures the complex coherence function of the electric field, $E$, between two points, $Q_1$ and $Q_2$:

$$\Gamma(Q_1,Q_2) = \langle E(Q_1,t)E^*(Q_2,t)\rangle_t \tag{1}$$

where $t$ is time, $E^*$ is the complex conjugate, and the pointed brackets indicate a time average. The coherence function is the Fourier transform of the sky brightness, $I(\mathbf{x})$ (*3*):

$$\Gamma(\mathbf{u}_1,\mathbf{u}_2) = \int_C I(\mathbf{x})e^{i(2\pi/\lambda)(\mathbf{u}_1-\mathbf{u}_2)\cdot\mathbf{x}}d\mathbf{x} \tag{2}$$

where $\mathbf{u}$ is the position vector from $Q$ as projected on a plane perpendicular to the line of sight, $\mathbf{x}$ is an angular Cartesian coordinate system centered on the object, and $C$ is the field of view of the array elements. [This is a special case of a more general expression (*3*).] Therefore, an interferometer measures a single Fourier coefficient of the sky brightness, with a spatial frequency dependent on the separation and orientation of the interferometer elements as seen from the object. Given samples of the fringe amplitude and phase for a number of configurations of an interferometer, one can make a structural determination by some form of model-fitting or, in the case of good sampling, form an image by direct Fourier synthesis. Hence phase-stable radio-interferometric arrays can image complex objects from measurements of the fringes at many different interferometer spacings. The actual image can be obtained by simple Fourier inversion of Eq. 2.

The construction of phase-stable radio interferometers was difficult during the 1950s, and so determinations of the structure of a celestial object could only be made from the amplitude of the fringes measured by the interferometer. Unfortunately, in many cases this lack of phase information leads to ambiguities in the determination of the structure, especially if the quality of the data recorded is poor. In 1958, Jennison (*2*) noted that in a network of three antennas, each pair of which formed an interferometer, a phase error at any given telescope vanishes in the sum of the fringe phases around the loop (see Fig. 2). To demonstrate this, note that the coherence phase measured between elements $i$ and $j$, $\Theta_{i,j}$, is related to the true coherence phase, $\hat{\Theta}_{i,j}$:

$$\Theta_{i,j} = \hat{\Theta}_{i,j} + \phi_i - \phi_j \tag{3}$$

where $\phi_i$ is the phase error associated with the $i$th element, and I have ignored additive noise. Jennison's sum of the phase around a loop, $\Phi_{ijk}$, is defined as

$$\Phi_{ijk} = \Theta_{i,j} + \Theta_{j,k} + \Theta_{k,i} \tag{4}$$

The true sum is similarly defined:

$$\hat{\Phi}_{ijk} = \hat{\Theta}_{i,j} + \hat{\Theta}_{j,k} + \hat{\Theta}_{k,i} \tag{5}$$

And so we have that the observed and true sums are equal:

$$\Phi_{ijk} = \hat{\Phi}_{ijk} \tag{6}$$

This is a very important result: it says that this sum is completely independent of the antenna-based phase errors and contains information about the structure of an object. This observed "closure phase" [so named by Rogers *et al.* (*4*)] can thus be used as a constraint upon a structural determination (*5*) under conditions where the actual coherence phase is totally corrupted.

Similar arguments can be made for the amplitude gain of an antenna, and "closure amplitudes" can be derived (*6, 7*). This technique is most useful at high frequencies for removing the effect of amplitude variations caused by the fluctuating absorption of the atmosphere.

Although closure phase was invented in the 1950s, it was not used in earnest until the mid-1970s. After Jennison's original paper, the problems of building short-spacing (up to a few kilometers) phase-stable interferometers were overcome by developments in electronics, and so closure phase was no longer quite so vital (*8*). This remained true until the advent of very long baseline interferometry (VLBI), which brought new problems that could not be solved by electronics alone. In VLBI, the interferometer elements are very widely separated, perhaps on different continents, and the signals are recorded on magnetic tape for subsequent measurement of the coherence. The unknown geometry (due to uncertainties in the coordinate systems) and timing (due to the absence of a single time standard common to all elements) prevent the accurate measurement of the true visibility phase. However, because these errors originate at antennas, Jennison's reasoning applies again, and the closure phase must be a good observable quantity (provided that the errors are not sufficiently large that fringe is lost completely).

Rogers *et al.* (*4*) were the first to apply closure phase to VLBI. A major obstacle to the use of closure phase was that it could not be used in an analytic inversion of the imaging Eq. 2. Instead, Rogers *et al.* used it as a constraint in a model-fitting structural determination of the radio sources 3C273 and 3C84. In subsequently developed imaging methods, the consistency of an estimate of the object with the measured closure phases was obtained with an iterative technique that incorporated a priori information about the object, such as finite size, and positivity of the brightness [see below and (*9*) for an account of this point]. As the number of antennas increased, the amount of information in the closure phases increased: for an array of $N$ elements, there are $N(N-1)/2$ independent fringe phases, and

$(N-1)(N-2)/2$ independent closure phases (*10*), so the deficit narrows as $N$ increases. Hence one can argue that for arrays of ten antennas, the closure phases contain 80% of the information available in the fringe phases.

Interferometric arrays of moderate baselines (up to some tens of kilometers) can be made phase-stable in the electronics by means of phase-locked oscillators (*3*), but another source of phase errors arises: the earth's atmosphere. The wave front is distorted by variations in the refractive index due, at low frequencies, to fluctuations in the electron content of the ionosphere, and at high frequencies, to fluctuations in the water vapor content of the troposphere (*3*). Here again, however, closure phase can be invoked to save the situation because the atmospheric effects are common to all baselines involving a given antenna and so their effect must vanish in the closure phases. Unfortunately, another, more mundane difficulty arises if the number of antennas in the array is large [for example, 27 antennas for the Very Large Array (VLA) (*11*); see Fig. 3]: the number of possible closure phases, $N(N-1)(N-2)/6$, is much greater than the number of independent closure phases, $(N-1)(N-2)/2$, and hence the logic of which closure phases to use in imaging becomes very involved. Complication of this sort is usually a sign that the formulation of a problem could be improved. Indeed, it was soon found that the closure phases could be best exploited by "self-calibration" imaging methods (*10, 12*), which permit only those changes to the measured coherence phases that leave the closure phases undisturbed.

## Self-Calibration

From the definition of closure phase, we can see that any change to the phase of a single antenna must leave the closure phase unaltered (*10*). Therefore, we can use the closure phase constraints in imaging simply by allowing the antenna phases, $\phi_i$, to be degrees of freedom in the estimation of the sky brightness. This idea has several advantages:

1) The closure phases are never actually calculated explicitly, nor need they be stored.

2) Additive receiver noise can be treated correctly by choosing the antenna phases to minimize the mean square misfit between the observed coherences and those predicted from some model, as modified by the (unknown) antenna phases:

$$S = \sum_{i,j} |\Gamma_{i,j} - e^{i\phi_i}e^{-i\phi_j}\hat{\Gamma}_{i,j}|^2 w_{i,j} \qquad (7)$$

The weight $w_{i,j}$ can be used to favor baselines $i,j$ that have good signal-to-noise ratios (SNRs) or to exclude those baselines where the model is known to make poor predictions (*10, 12*).

3) The antenna phases, once calculated by self-calibration, can be used as estimates for the calibration of a nearby object. This reflects a subtle shift in the technique: closure phases are constructed to avoid the effects of the antenna phase errors, whereas in self-calibration the phase errors are calculated explicitly (see below).

A flow chart of a typical self-calibration algorithm is shown in Fig. 4. The extra freedom allowed in the antenna phases must, of course, be counterbalanced in some way, so that there remain more constraints than degrees of freedom. There are two approaches: first, by using certain restrictive assumptions about the object being imaged or, second, by using an array with some redundancy of measurement (*13*). In the flow chart shown, a priori information about the object is used in the step that converts an image of the sky into a model of the object. This stage usually consists of the rejection of parts of the image that have negative brightness or lie outside a window, within which the true object is known to lie. Figure 5 shows the images obtained before and after self-calibration for a typical VLA observation.

The most important limitation of self-calibration is that the measurements of the coherence phase must have SNRs greater than unity in the atmospheric coherence time. This is required because the antenna phases are actually estimated from the measurements.

Once the concept of self-calibration is understood, it is easy to see how it can be generalized to other situations. For example, in VLBI not only is it important to determine the antenna phase, but the first derivatives are also of interest. These derivatives, that with respect to time being known as the fringe rate and that with respect to frequency corresponding to a delay error, reflect principally errors in the assumed geometry and timekeeping of the interferometers. Self-calibration can easily be extended to cover this case (*14*). Another interesting extension of self-calibration is in overcoming the nonisoplanatic nature of the ionosphere at low frequencies ($\ll$ 1 GHz). In nonisoplanatic conditions, the phase error at any given antenna varies over the field of view, and so simple closure phases are no longer invariant to these errors. Schwab has noted that, by allowing the phase error to be described by a small number of degrees of freedom, imaging may still be possible (*15*). This last example is

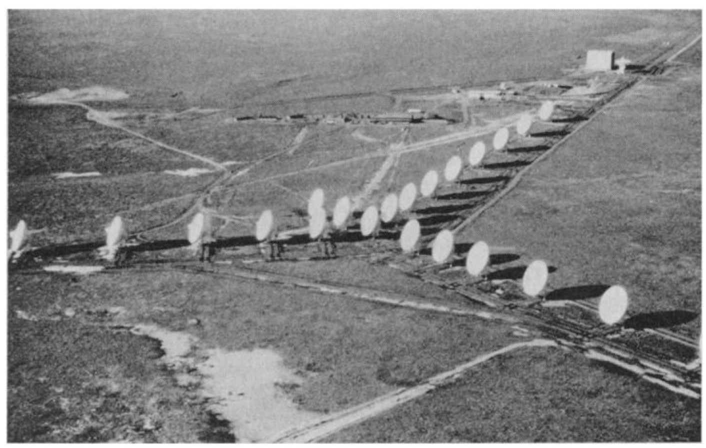

**Fig. 3.** The Very Large Array radio-interferometric telescope on the Plains of San Agustin, New Mexico, consists of 27 radio telescopes, each 25 km in diameter, that can be configured to sample baselines ranging from about 25 m up to 35 km.

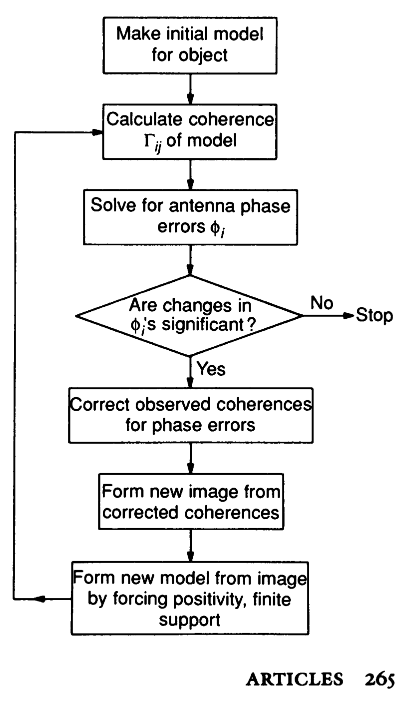


**Fig. 4.** Flow chart for the self-calibration process.

particularly interesting because it represents an application for which it is difficult to derive a quantity analogous to closure phase.

Self-calibration is now a very important part of imaging techniques at radio wavelengths. Imaging of any sort in VLBI requires self-calibration, whereas in connected-element radio interferometry high-quality imaging is made possible only by the combination of carefully designed electronics for the correlation of the electric field samples together with self-calibration (*16*). The best images have dynamic range [ratio of the peak brightness to the root-mean-square (rms) background noise] approaching $10^6$. Figure 6 shows a self-calibrated image of a complex object: the innermost 20 arc seconds of the elliptical galaxy M87 (*17*). This image, which was made from observations with the National Radio Astronomy Observatory VLA, has a dynamic range approaching 50,000. Without self-calibration techniques, the dynamic range of this image would be limited by the errors in an external calibration to no more than about 100. Only the brightest point, the galaxy nucleus, would then be visible.

We may contrast the two strategies of closure phase and self-calibration as schemes of cancellation and of correction. The closure phase is an observable quantity in which instrumental effects cancel, whereas in self-calibration the instrumental effects are estimated and corrected.

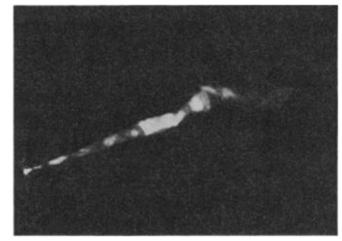

**Fig. 6.** A typical self-calibrated radio image of the jet in the elliptical galaxy M87 made with the VLA observing at a wavelength of 2 cm (*17*). The dynamic range is about 50,000, which is about 500 times better than that possible via external calibration. The full field of view is about 30 arc seconds (1 arc second ~250 light-years), and the resolution is about 0.15 arc second. Before self-calibration only the brightest point in the image (the galaxy nucleus) is visible. The artifacts north and south of the galaxy nucleus are due to errors in the VLA, which do not factor per element.

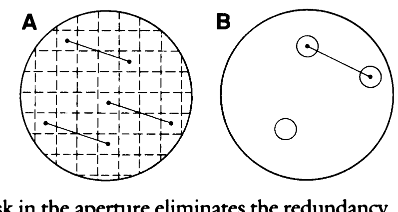


**Fig. 7.** Redundancy in the aperture of a conventional optical telescope. (**A**) A continuous aperture split into a grid of imaginary patches, each of which is the size of the atmospheric coherence scale. A given interferometer spacing is measured many times. (**B**) A mask in the aperture eliminates the redundancy. Although the mask shown here is very simple, quite complex nonredundant masks can be used (*23*).

## Optical Imaging

In optical imaging, the earth's atmosphere limits the resolving power of a telescope to that of a 10- to 20-cm aperture, because, on propagation through the troposphere, an optical wavefront will suffer phase perturbations with a characteristic size scale of about 10 to 20 cm and a characteristic time scale of about 10 to 50 ms (*18*). On time-averaging over many seconds, the effect of the phase errors is to produce the "seeing disk," which has a characteristic angular size of about 1 arc second. There are two main ways around this limit: either find some measurable quantity that is invariant to the phase errors or find a way of calculating and removing the phase errors.

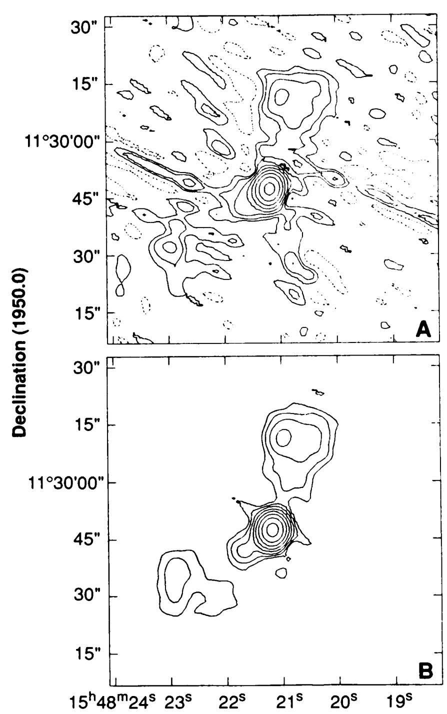


**Fig. 5.** An example of the self-calibration of an observation made with the VLA. (**A**) The best image obtained without self-calibration. There are spurious features at the level of 1% of the peak brightness. (**B**) The same image after self-calibration of the antenna phases. The level of spurious detail has decreased to 0.3% of the peak brightness. The lowest contour level in both (A) and (B) is 0.6%. [Adapted from (*11*) by permission, copyright 1983 IEEE]

I will discuss the former approach first. One can easily apply closure phase to optical imaging by forcing the optical aperture to mimic the sparse filling found in radio interferometry. We can consider the aperture of a conventional optical telescope to be composed of many interferometers formed between patches of constant atmospheric phase (see Fig. 7). An image at the focal plane of a telescope is made from the combination of all these individual interferometers. Although these virtual interferometers give very redundant measurement of some spacings, atmospheric phase errors cause these redundant samples to have differing phases. Hence, even given a short exposure image in which the atmosphere is frozen, it is not possible to untangle the contributions of the individual interferometers. Because the redundancy of the aperture is responsible for this difficulty, the answer is to use a mask in the pupil to force nonredundancy of measurement. It is then possible to derive closure phases from the Fourier transform of a single short snapshot (*19–22*). A number of groups are now engaged in this type of optical imaging. Figure 8 shows an image provided by the Caltech group lead by S. R. Kulkarni. This image of a binary star was constructed from a series of measurements of closure phases with various configurations of the mask holes (*23*).

The major disadvantage of the masking approach is that most of the incident photons are lost. For weak objects, another complementary set of methods is therefore preferred; these are based on the existence of "speckles." Over the years many observers had noted that for very brief periods of time, fine detail (the speckles) could be seen in the seeing disk (see Fig. 9). Labeyrie (*24*) was the first to suggest a way of using this information systematically. He noted that, from averages of the power spectrum of short exposure images of the seeing disk, it is possible to obtain the power spectrum of the astronomical object, distorted by a seeing-dependent modulation transfer function that could be calibrated on a nearby star. Averaging the power spectrum discards the corrupted phase information, and so Labeyrie's method is limited to imaging simple objects for which the Fourier phase information is unimportant.

Because averaging of the power spectrum is equivalent to averaging the autocorrelation of the snapshot images, it seems reasonable to believe that more information can be extracted from higher order correlation functions. In confirmation, Weigelt and Wirnitzer (*25*) showed that from averages of the triple-correlation function it is possible to recover most of the Fourier phase information and thus image complicated objects. [Knox and Thompson (26) developed a simpler and competitive scheme for extracting phase information from gradient information.] Because this procedure preserves some of the phase information, one might expect it to be related to Jennison's phase closure method. This was recently shown to be correct (27, 28). Weigelt's method is in fact a generalization of closure phase to filled apertures such as optical telescopes and also to low SNR. The key advantage is that all the incident photons can be used.

As we have seen in radio interferometry, the other possible countermeasure to a source of errors in a system is to estimate and correct the errors. This approach has also been tried in optical imaging. The phase errors introduced by the atmosphere can be corrected in real time by adjusting the profile of a "rubber mirror" (29, 30). The rubber mirror has independently movable segments approximately the size of each dashed rectangle (Fig. 7A). The most important issue is how best to control this mirror to get a good image. There are two principal possible approaches: first, by using a servo-loop in which the image "sharpness" is maximized, or, second, by measuring directly the phase perturbations across the pupil of the instrument. In sharpness-maximization adaptive optics, the mirror is controlled to optimize a quantity that is related to the image quality, such as the image dispersion. Hamaker *et al.* (31) showed that maximizing the image dispersion is equivalent to requiring that all redundant measurements of a given spatial frequency must yield the same phase. Sharpness maximization is difficult in practice because the optimization of the figure of the mirror must take place within an atmospheric coherence time, typically 10 ms. Hence a typical mirror with many elements must be driven very fast in order to complete the optimization. Furthermore, the SNR in that time is inevitably poor.

A better approach is to measure the phase perturbations across the pupil. There are a number of schemes for performing this measurement (32). One of the simplest uses the Shack-Hartmann sensor to measure the tilt of the wave front across the spatial dimension of one atmospheric coherence cell and integrate these tilts spatially to get the full phase perturbation. Typically some fraction of the incident light is siphoned off for monitoring of the phase perturbations. A particularly exciting possibility is the use of artificial stars created by exciting the sodium layer in the upper atmosphere with a high-power laser (33, 34).

To complete our cross-linking, I will now discuss the intimate relationship between adaptive optics and the self-calibration principle. In sharpness-optimization adaptive optics, the rubber mirror is reshaped to produce the highest quality image, just as in radio interferometry the calibration of the array is allowed to vary so as to produce an acceptable and self-consistent image. We can immediately say that because only the pupil phase is allowed to vary, adaptive optics must maintain the closure phases; therefore, objects that differ in their closure phases cannot be confused by sharpness-optimization adaptive optics.

## Focal-Plane Self-Calibration

The phase-correction schemes described in the previous section work principally in the focal plane, from the intensity of the image alone, either statistically as in speckle imaging or from a single image with adaptive optics. However, the radiation at the focal plane of a telescope also has some coherence structure that could, in principle, be measured and utilized in phase correction. It has recently been shown that from measurements of the coherence function of the radiation in the focal plane it is possible to derive both the structure

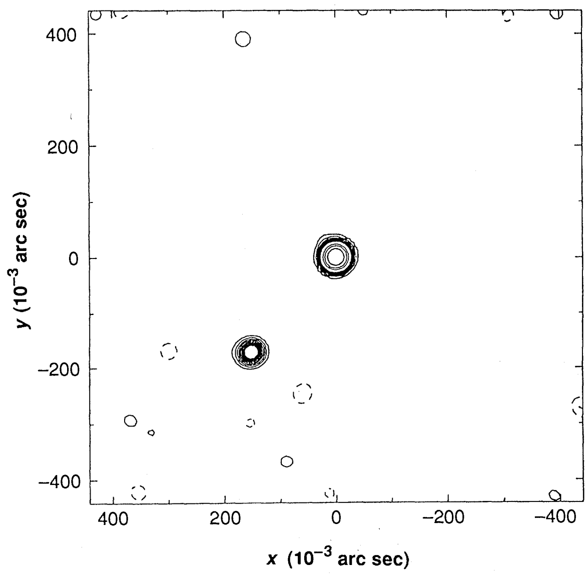


**Fig. 8.** An example of an image of β Corona Borealis formed from closure phases measured with a mask in the aperture of the Palomar 200-inch telescope. The optical magnitude of the star is $m_v = 3.7$. The resolution is 0.230 arc second. [Adapted from (23) by permission of the American Astronomical Society]

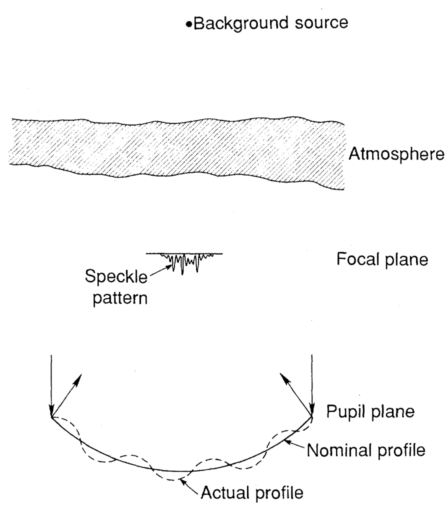


**Fig. 9.** Sources of phase errors in telescopes. Two main types of error affect single-dish telescopes, phase errors due to the atmosphere (usually dominant at optical wavelengths) and phase errors due to deviation of the reflector from the nominal profile (usually dominant at radio wavelengths). Both types of errors induce "speckles" in the short-integration image.

of the object and an estimate of the phase errors by means of a procedure that is a focal-plane analog of the self-calibration schemes described above (35, 36).

Although the objects being imaged in astronomy nearly always emit incoherently, an image itself is partially coherent. There are two causes of this coherence. (i) The finite size of the aperture means that the radiation in the focal plane must be coherent over scale size $\sim F\lambda/D$, where $F$ is the focal length and $D$ is the diameter of the telescope. (ii) Phase errors of characteristic scale size $d$ must scatter radiation into regions in the focal plane of scale size $F\lambda/d$. The first type of coherence is obviously fundamental, arising as it does from diffraction. However, the second type of coherence can be used to provide information about the phase errors.

The focal-plane coherence function, $\Gamma(\mathbf{p}_1,\mathbf{p}_2)$, is given by a double Fourier transform of the effective pupil-plane coherence function, $\Gamma(\mathbf{u}_1,\mathbf{u}_2)$:

$$\Gamma(\mathbf{p}_1,\mathbf{p}_2) = \frac{1}{\lambda^2}\iint\Gamma(\mathbf{u}_1,\mathbf{u}_2)e^{i(2\pi/F\lambda)(\mathbf{p}_1\cdot\mathbf{u}_1-\mathbf{p}_2\cdot\mathbf{u}_2)}d\mathbf{u}_1 d\mathbf{u}_2 \quad (8)$$

The effective pupil-plane coherence function is related to the actual coherence function:

$$\Gamma(\mathbf{u}_1,\mathbf{u}_2) = e^{j\phi(\mathbf{u}_1)}e^{-j\phi(\mathbf{u}_2)}\hat{\Gamma}(\mathbf{u}_1 - \mathbf{u}_2) \tag{9}$$

In conventional pupil-plane self-calibration, the pupil-plane coherence function is measured directly and redundancy of measurement can be used to derive both the phase errors and the true pupil-plane coherence function. The principal innovation in focal-plane self-calibration is that the pupil-plane coherence function is obtained from a Fourier transform of the focal-plane coherence function. Then self-calibration proceeds as usual but with redundancy of measurement assured. Cornwell and Napier (*36*) described focal-plane self-calibration in more detail and showed some numerical simulations.

## Scattering and Coherence

Although coherence-measuring focal-plane arrays do not yet exist, some of the predictions of the theory in the previous section can be tested with a radio-interferometric array such as the VLA in the focal plane of a well-chosen lens. The most obvious candidate for such a lens at radio wavelengths is the solar wind. This is a flow of plasma that moves outward from the sun at velocities up to 400 km/s (Fig. 10). Fluctuations in the electron density cause rapid scintillation of a background object seen through the wind (*37*). Cornwell *et al.* (*38, 39*) used the VLA to image the scattered radiation with high time (40 ms) and high angular (0.1″) resolution. Radiation is scattered toward the observer from a finite region within the solar wind, which can for some purposes be thought of as a thin screen. On propagation to the earth, the radiation can be thought of as undergoing a Fourier transform just as would occur at the focal plane of a conventional lens (*40*). This result is slightly counterintuitive, because it suggests a special alignment of the source, screen, and the earth although none is apparent from the geometry. The key requirement that resolves this conceptual difficulty is that the scattering must be very strong: that is, rays of the scattered radiation must cross far before reaching the earth. Given complete sampling of the effective focal plane and following the arguments of the previous section, it should then be possible to estimate both the object and the scattering screen.

The main obstacle to this proposal is that an array such as the VLA permits only sparse sampling of the coherence function. One way of understanding this problem is to note that at the focal plane of a real telescope, it is necessary to obtain the coherence between every pair of points. However, in conventional radio interferometry, the objects being imaged are incoherent and so sampling of the coherence between every pair of points is unnecessary. Consequently, modern arrays are designed to sample antenna separations rather than antenna positions. Arrays that have uniformly spaced elements are called redundant because any one spatial frequency of the object is measured many times. Self-calibration of such redundant arrays is particularly simple because the redundancy of measurement can be used to derive the antenna phases.

In the case of a radio-interferometric array observing a scattering disk, the object being imaged is coherent and so sampling of separations alone is insufficient. For scattering of a background point object, the coherence function measured for short integrations ($\sim$10 to 40 ms) can be factored into parts dependent purely upon position:

$$\Gamma(\mathbf{u}_1,\mathbf{u}_2) = Sg(\mathbf{u}_1)g^{*}(\mathbf{u}_2) \tag{10}$$

where $S$ is the strength of the background object (*39*). The function $g(\mathbf{u})$ represents an effective modulation of the antenna gain by the scattering process. In the example of scattering in the solar wind, this relation is indeed maintained to very good accuracy.

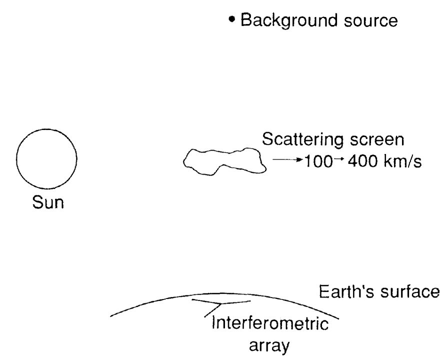


**Fig. 10.** Schematic of scattering induced by solar wind. Fluctuations in the electron density along the line of sight to the source cause a scattering of radiation. For some purposes this can be thought of as a lens, and so speckles can be seen on the earth's surface (*39*).

The results of Cornwell *et al.* (*39*) show that the scattering of radio waves in the solar wind can be investigated by applying the theory of focal-plane self-calibration. Cornwell *et al.* demonstrated coherence of the scattered radiation and also described how high-resolution imaging may be possible. One version of their test for coherence is to measure the closure quantities of the measured coherence function because, according to Eq. 10, the closure phase must be zero and the closure amplitude must be unity.

## Discussion

We are now in a position to see just why methods based on the closure phase can work. One of the results of the previous section was that the closure phase of a completely coherent object is always zero or alternatively that the measured coherence function factors perfectly into two position-dependent parts. Remember now that in self-calibration, the position-dependent part of the pupil-plane coherence function is allowed to vary. Clearly, in the case of a coherent object, such as that corresponding to scattered radiation seen with high time resolution, the result of such self-calibration must be a point object. Hence, self-calibration methods assume incoherence of the emitting object and are completely insensitive to any coherent emission processes. This last point demonstrates most clearly just what information about the object is lost by the use of self-calibration techniques. Fortunately, in most astronomical imaging, it makes sense to trade blindness to coherent emission for increased image quality.

The driving force behind Jennison's closure phase is that the imaging performed by all telescopes is based on correlation of the radiation field, and so one measures many more numbers than there are sources of error. For example, an $N$-element interferometric array measures $O(N^2)$ independent numbers: the coherence function between the radiation field measured at the sensors. Hence any sensor-based errors are fewer in number than the number of measurements. (An exception to this occurs when the measured numbers are not independent, as occurs for a coherently emitting source.) A conventional, image-forming telescope can also be thought of as a correlation device (*27*), subject to pupil plane–based phase errors. In all these cases, after subtracting the errors, we are left with some good observables. The closure phases are one example of these quantities, and self-calibration is one procedure for using the closure phases in imaging.

Closure phase methods are therefore applicable to any instrument that measures correlations between the quantities measured by error-prone sensors. The closure phase principle underlies imaging in many different astronomical contexts: radio interferometry, high-resolution imaging with single optical telescopes, aberration correction in single radio telescopes, and scintillation phenomena. I hope that the successes of such methods in astronomy will encourage others to try a similar approach in other imaging fields.

REFERENCES AND NOTES

1. M. Ryle, *Proc. R. Soc. London Ser. A* **211**, 351 (1952).
2. R. C. Jennison, *Mon. Not. R. Astron. Soc.* **118**, 276 (1958).
3. A. R. Thompson, J. M. Moran, G. W. Swenson, *Interferometry and Synthesis in Radio Astronomy* (Wiley-Interscience, New York, 1986).
4. A. E. E. Rogers *et al.*, *Astrophys. J.* **193**, 293 (1974).
5. R. C. Jennison and V. Latham, *Mon. Not. R. Astron. Soc.* **119**, 174 (1959).
6. F. G. Smith, *Proc. Phys. Soc. London Sect. B* **65**, 971 (1952).
7. R. Q. Twiss, A. W. L. Carter, A. G. Little, *Observatory* **80**, 153 (1960).
8. R. D. Ekers, in *Proceedings of the National Radio Astronomy Observatory Workshop on "Serendipitous Discoveries in Astronomy,"* K. I. Kellerman and B. Sheets, Eds. [National Radio Astronomy Observatory (NRAO), Green Bank, WV, 1984], p. 154.
9. A. C. S. Readhead and P. N. Wilkinson, *Astrtophys. J.* **223**, 25 (1978).
10. T. J. Cornwell and P. N. Wilkinson, *Mon. Not. R. Astron. Soc.* **196**, 1067 (1981).
11. P. J. Napier, R. T. Thompson, R. D. Ekers, *Proc. IEEE* **71**, 1295 (1983).
12. F. R. Schwab, *Proc. Soc. Photo-Opt. Instrum. Eng.* **231**, 18 (1980).
13. J. E. Noordam and A. G. de Bruyn, *Nature* **299**, 597 (1982).
14. F. R. Schwab and W. D. Cotton, *Astron. J.* **88**, 688 (1983).
15. F. R. Schwab, *ibid.* **89**, 1076 (1984).
16. R. A. Perley, in *Proceedings of Synthesis Imaging Workshop, Socorro, 1985*, R. A. Perley, F. R. Schwab, A. H. Bridle, Eds. (NRAO, Green Bank, WV, 1986), p. 161.
17. F. N. Owen, P. E. Hardee, T. J. Cornwell, *Astrophys. J.*, in press.
18. N. J. Woolf, *Annu. Rev. Astron. Astrophys.* **20**, 367 (1982).
19. D. H. Rogstad, *Appl. Opt.* 7, 585 (1968).
20. W. T. Rhodes and J. W. Goodman, *J. Opt. Soc. Am.* **63**, 647 (1973).
21. A. H. Greenaway, *Opt. Commun.* **42**, 157 (1983).
22. C. A. Haniff *et al.*, *Nature* **328**, 694 (1987).
23. T. Nakajima *et al.*, *Astron. J.* **97**, 1510 (1989).
24. A. Labeyrie, *Astron. Astrophys.* **6**, 85 (1970).
25. G. Weigelt and B. Wirnitzer, *Opt. Commun.* **21**, 55 (1977).
26. K. T. Knox and B. J. Thompson, *Astrophys. J.* **193**, L45 (1974).
27. F. Roddier, *Opt. Commun.* **60**, 145 (1986).
28. T. J. Cornwell, *Astron. Astrophys.* **180**, 269 (1987).
29. A. Buffington, F. S. Crawford, S. M. Pollaine, C. D. Orth, R. A. Muller, *Science* **200**, 489 (1978).
30. R. A. Muller and A. Buffington, *J. Opt. Soc. Am.* **64**, 1200 (1974).
31. J. P. Hamaker, J. D. O'Sullivan, J. E. Noordam, *ibid.* **67**, 1122 (1977).
32. F. Merkle, in *Proceedings of the Second Workshop on "ESO's Very Large Telescope,"* S. D'Odorico and J.-P. Swings, Eds. (European Southern Observatory, Garching, West Germany, 1986), p. 443.
33. R. Foy and A. Labeyrie, *Astron. Astrophys.* **152**, L29 (1985).
34. L. A. Thompson and C. S. Gardner, *Nature* **328**, 229 (1987).
35. T. J. Cornwell and P. J. Napier, in *Proceedings of the National Radio Astronomy Observatory Workshop on "Radio Astronomy from Space,"* K. W. Weiler, Ed. (NRAO, Green Bank, WV, 1987), p. 215.
36. ———, *Radio Sci.* **23**, 739 (1988).
37. J. P. Jokipii, *Annu. Rev. Astron. Astrophy.* **11**, 1 (1973).
38. T. J. Cornwell, K. R. Anantharamaiah, R. Narayan, in *Proceedings of the San Diego Workshop on "Radio Wave Scattering in the Interstellar Medium,"* J. Cordes, B. J. Rickett, D. C. Backer, Eds. (American Institute of Physics, New York, 1988), p. 92.
39. ———, *J. Opt. Soc. Am.*, in press.
40. J. W. Goodman, *Fourier Optics* (Wiley, New York, 1975).
41. This article gives my personal view of the evolution of closure phase in astronomy, a view that has been strongly influenced by discussions over the last 10 years with many of my co-workers in this field. In addition to thanking the general community, I also thank specifically the following collaborators for fruitful discussions about closure phase: P. N. Wilkinson, G. Weigelt, P. J. Napier, K. R. Anantharamaiah, R. Narayan, and R. D. Ekers. I thank F. Owen and P. Hardee for permission to show the M87 image and T. Nakajima for permission to show the image of β Corona Borealis. I also thank two anonymous referees for comments on an earlier version of this article. Associated Universities Inc. operates the National Radio Astronomy Observatory under National Science Foundation Cooperative Agreement AST-8814515.

# The Rat as an Experimental Animal

THOMAS J. GILL III,* GARRY J. SMITH, ROBERT W. WISSLER, HEINZ W. KUNZ

**The development and characterization of many inbred, congenic, and recombinant strains of rats in recent years has led to the detailed genetic description of this species, especially in regard to its major histocompatibility complex. This information has contributed substantially to the study of comparative genetics and has greatly enhanced the utility of the rat in a variety of areas of biomedical research. This article focuses on the use of the rat in immunogenetics, transplantation, cancer-risk assessment, cardiovascular diseases, and behavior.**

THE RAT IS A MAJOR EXPERIMENTAL ANIMAL IN TRANSPLANTATION, immunology, genetics, cancer research, pharmacology, physiology, neurosciences, and aging. The strains and randomly bred stocks that have been used almost exclusively are derived from the Norway rat (*Rattus norvegicus*), which is thought to have originated in the area between the Caspian Sea and Tobolsk, extending as far east as Lake Baikal in Siberia. It spread to Europe and the United States with the development of commerce in the 18th century, and by the middle of the 19th century it was being used extensively for studies in anatomy, physiology, and nutrition. The first inbred lines were developed at the beginning of the 20th century by H. H. Donaldson, W. E. Castle, and their colleagues for studies in basic genetics and in cancer research (*1*). Further development and genetic characterization of inbred, congenic, and recombinant strains occurred in the United States, Japan, and Czechoslovakia (*2*), and several reviews have documented these developments in detail (*3–5*). In addition to its experimental uses, the rat has a worldwide economic and medical impact, since it destroys one-fifth of the world's crops each year, carries many diseases that are pathogenic for humans, and kills many children by direct attack (*6*).

This review will focus on current work utilizing the rat in immunogenetics, transplantation, cancer-risk assessment, cardiovascular diseases, and behavior. In these areas of research, the rat has the advantage of being a well-characterized, intermediate-sized rodent without the disadvantages, both scientific and economic, of larger animals and without many of the technical disadvantages of smaller rodents.

T. J. Gill III is the Maud L. Menten Professor of Experimental Pathology and professor of human genetics and H. W. Kunz is associate professor of pathology at the University of Pittsburgh School of Medicine, Pittsburgh, PA 15261. G. J. Smith is associate professor and director of the Carcinogenesis Research Unit at the School of Pathology of the University of New South Wales, Kensington, New South Wales, 2033 Australia. R. W. Wissler is the Donald N. Pritzker Distinguished Service Professor of Pathology, active emeritus, at the University of Chicago School of Medicine, Chicago, IL, 60637.

*To whom correspondence should be addressed.